BIOCHEMISTRY
including biophysical chemistry & molecular biology

Article

pubs.acs.org/biochemistry

Key Residues Regulating the Reductase Activity of the Human Mitochondrial Apoptosis Inducing Factor

Raquel Villanueva,[†,‡] Patricia Ferreira,[*,†,‡] Carlos Marcuello,[§] Alejandro Usón,[†] M. Dolores Miramar,[†] M. Luisa Peleato,[†,‡] Anabel Lostao,[§,∥] Santos A. Susin,[⊥,#,∇] and Milagros Medina[*,†,‡]

[†]Departamento de Bioquímica y Biología Molecular y Celular, Facultad de Ciencias, [‡]Instituto de Biocomputación y Física de Sistemas Complejos, and [§]Laboratorio de Microscopias Avanzadas, Instituto de Nanociencia de Aragón, Universidad de Zaragoza, 50009 Zaragoza, Spain

[∥]Fundación ARAID, 50018 Zaragoza, Spain

[⊥]INSERM U1138, Cell Death and Drug Resistance in Lymphoproliferative Disorders Team, Centre de Recherche des Cordeliers, F-75006, Paris, France

[#]Université Pierre et Marie Curie-Sorbonne Universités, F-75006, Paris, France

[∇]Université Paris Descartes-Sorbonne Paris Cité, F-75006, Paris, France

ABSTRACT: The human Apoptosis Inducing Factor (hAIF) is a bifunctional NAD(P)H-dependent flavoreductase involved in both mitochondrial energy metabolism and caspase-independent cell death. Even though several studies indicate that both functions are redox controlled by NADH binding, the exact role of hAIF as a reductase in healthy mitochondria remains unknown. Upon reduction by NADH, hAIF dimerizes and produces very stable flavin/nicotinamide charge transfer complexes (CTC), by stacking of the oxidized nicotinamide moiety of the NAD^+ coenzyme against the *re*-face of the reduced flavin ring of its FAD cofactor. Such complexes are critical to restrict the hAIF efficiency as a reductase. The molecular basis of the hAIF reductase activity is here investigated by analyzing the role played by residues contributing to the interaction of the FAD isoalloxazine ring and of the nicotinamide moiety of NADH at the active site. Mutations at K177 and E314 produced drastic effects on the hAIF ability to retain the FAD cofactor, indicating that these residues are important to set up the holo-enzyme active site conformation. Characterization of P173G hAIF indicates that the stacking of P173 against the isoalloxazine ring is relevant to determine the flavin environment and to modulate the enzyme affinity for NADH. Finally, the properties of the F310G and H454S hAIF mutants indicate that these two positions contribute to form a compact active site essential for NADH binding, CTC stabilization, and NAD^+ affinity for the reduced state of hAIF. These features are key determinants of the particular behavior of hAIF as a NADH-dependent oxidoreductase.

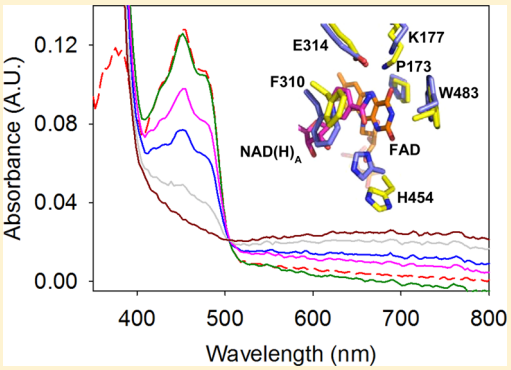

The Apoptosis Inducing Factor (AIF) is a FAD-containing protein confined to mitochondria in healthy cells where it exerts a vital but still not well described function in bioenergetics and redox metabolism.[1−4] After an apoptosis-related mitochondrial outer membrane permeabilization, AIF is translocated to the cytosol and subsequently to the nucleus where it contributes to chromatinolysis associated with the caspase-independent mode of programmed cell death.[5,6] The human AIF (hAIF) precursor is composed of an N-terminal mitochondrial localization sequence (aa 1−55), a transmembrane region (aa 66−84), and three soluble structural domains:[7] the FAD (aa 128−262 and 401−480) and NADH (aa 263−400) binding domains provide hAIF with a NAD(P)H-dependent reductase activity,[8] while the C-terminal domain (aa 481−613) is considered the pro-apoptotic domain of the protein[9−11] (containing a Pro-rich motif (aa 543−554) and a PEST sequence (aa 528−559)).[12,13]

Crystal structures have been reported for the soluble portions of hAIF and murine AIF (mAIF), both in the free FAD_{ox} and in the coenzyme-bound FAD_{rd} states, namely AIF_{ox} and AIF_{rd}:NAD(H) $hAIF_{\Delta 1-102\ rd}$:2NAD(H).[6,7,12−14] In the $hAIF_{\Delta 1-102\ rd}$:2NAD(H) structure two NAD(H) molecules were bound to the protein monomer (named $NAD(H)_A$ and $NAD(H)_B$). $NAD(H)_A$ in $hAIF_{\Delta 1-102\ rd}$:2NAD(H) and the single NAD^+ molecule in $mAIF_{rd}$:NAD^+ occupied the same position, which to date is the one related to the AIF NADH-reductase function.[12−14] $NAD(H)_A$ shows an extended conformation stabilized through an extensive H-bond network (G308, F310, L311, E314, E336, G399, E453, H454, and W483 residues, hAIF numbering). $NAD(H)_A$ binding induces

Received: June 21, 2015
Revised: July 30, 2015
Published: August 3, 2015

DOI: 10.1021/acs.biochem.5b00696
Biochemistry 2015, 54, 5175−5184

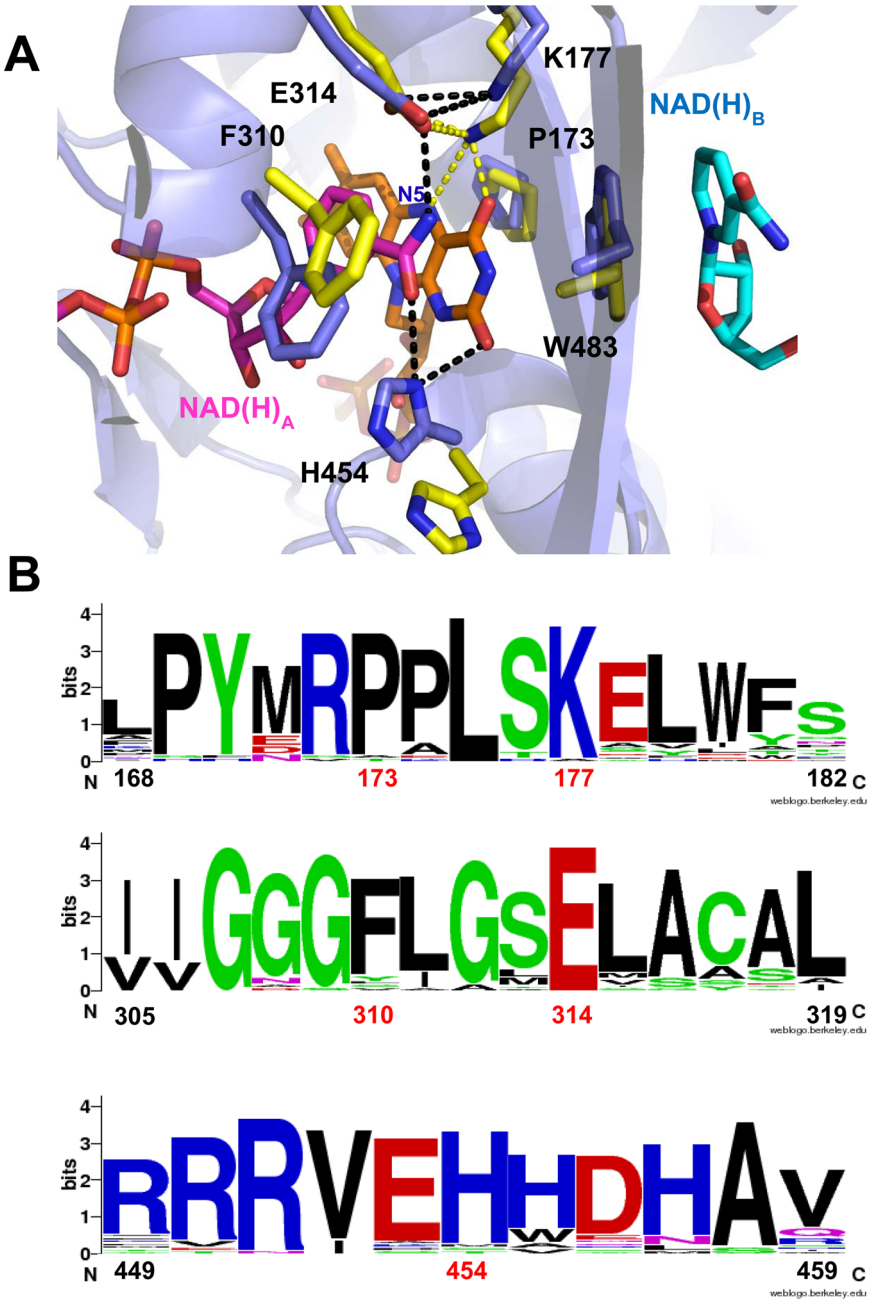

Figure 1. Isoalloxazine flavin ring environment in $hAIF_{\Delta 1-102}$. (A) Detail of the $hAIF_{\Delta 1-102\ rd}$:2NAD(H) complex (pdb 4BUR). FAD, $NAD(H)_A$, and $NAD(H)_B$ are shown as sticks and CPK colored in orange, pink, and blue, respectively. Side chains for key residues are shown as CPK colored violet sticks. Equivalent positions in $hAIF_{\Delta 1-121ox}$ are shown as yellow CPK colored sticks (pdb 4BV6). Key H-bonds in the $hAIF_{\Delta 1-102\ rd}$:2NAD(H) complex are shown as black dashed lines, and those for $hAIF_{\Delta 1-121ox}$ as yellow dashed lines. (B) Sequence logo for AIF sequences from different organisms and other related proteins (FR, BphA4, AMID, and MDAR) corresponding to the sequences including the mutated residues of hAIF. Multiple sequence alignments were performed with CLUSTALW2 program. Numbering corresponds to hAIF residues.

displacement of K177, F310, and H454 at the active site. The nicotinamide ring of $NAD(H)_A$ stacks between the F310 side chain and the *re*-face of the isoalloxazine in a conformation that appears optimal for charge transfer (Figure 1A),[12,14] while its amide group forms H-bonds with residues E314 and H454. In the oxidized protein, the K177 side-chain forms a H-bond with the N5 of the isoalloxazine flavin ring, whereas such H-bond breaks upon coenzyme binding and hydride transfer (HT) due to the slight displacement of the K177 side chain. Nevertheless, E314 contributes to place the K177 side chain in the oxidized as well as in the reduced structures. In both states, P173, at the N-terminal of the 173−180 α-helix, stacks against the pyrazine ring at the *si*-face of the flavin, whereas W483 T-stacks against the flavin pyrimidine ring. The second NAD(H) molecule ($NAD(H)_B$), identified in the $hAIF_{\Delta 1-102\ rd}$:2NAD(H) complex, stacks its nicotinamide against one of the sides of W483 (that on the other side stacks at the *si*-side of the flavin) (Figure 1A). Binding of $NAD(H)_B$ has been related to the redox reorganization of two specific insertions in the apoptotic domain of mammalian AIF (the 190−202 β-hairpin and the 509−560 segment).[14] Moreover, upon NADH binding and reduction, the enzyme undergoes dimerization.[12−14] $NAD(H)_A$

DOI: 10.1021/acs.biochem.5b00696
Biochemistry 2015, 54, 5175−5184

and NAD(H)$_B$ functions have been mainly elucidated from structural information, and therefore, further studies are required to establish the roles they play, as well as whether both of them have catalytic or mechanistic relevance. Thus, the available functional and structural data lead to the hypothesis that the apoptotic and the reductase activities of AIF might be regulated by NAD(H) binding in response to its availability in the environment.[14]

In the present study, we have aimed to better understand the molecular basis of the role of the NAD(H)$_A$ site of hAIF in its NADH-reductase activity. Thus, we analyze the specific function of some residues, namely, P173, K177, F310, E314, and H454, which contribute to fit the isoalloxazine ring and the nicotinamide ring of NAD(H)$_A$. These residues are fully conserved among AIF from different organisms (vertebrates and invertebrates) and highly conserved in several related proteins including biphenyl 2,3-dioxygenase ferredoxin reductase subunits (BphA4), enzymes of the glutathione reductase family, and oxygenase-coupled NADH-dependent ferredoxin reductases (Figure 1B), supporting the idea that they must have a role in the binding or even in the HT itself.[15,16] Noticeably, F310 and H454 are not highly conserved in AIF-related proteins, so they are less conserved overall. Our mutational analysis indicates that the highly conserved P173, K177, and E314 residues are required for FAD incorporation, while F310 and H454 are important for pyridine nucleotide binding, CTC stabilization, as well as to determine the typical *in vitro* low catalytic efficiency of AIF proteins to accept a hydride from NADH.

MATERIALS AND METHODS

Expression and Purification of hAIF$_{\Delta 1-102}$ Mutants. The P173G, K177W, F310G, E314S, and K177W/E314S hAIF$_{\Delta 1-102}$ mutants were obtained by site-directed mutagenesis using *Pfu* DNA polymerase from Stratagene. hAIF$_{\Delta 1-102}$ cDNA was cloned into the pBSK vector and used as template for PCR reactions with the following forward oligonucleotides bearing mutations (underlined) at the corresponding triplets (**bold**): P173G, 5′-CCGTACATGCGA**GG**TCCTCTTTCAAAAGAACTGTGG-3′; K177W, 5′-CCGTACATGCGACCTCCTCTTTCA**TGG**GAACTGTGGTTTTCAGATGACCC-3′; F310G, 5′-ATTACGATTATCGGTGGGGGC**GG**CCTTGGTAGCGAACTGGCCTGTG-3′; and E314S, 5′-GTGGGGGCTTCCTTGGTAGC**TGC**CTGGCCTGTGCTCTTGG-3′. The mutations were confirmed by sequence analysis (ABIPrism 3100, Applied Biosystems, CNIO, Madrid). The cDNA encoding for the corresponding hAIF$_{\Delta 1-102}$ mutants was cloned into the pET28a expression vector with a cleavable N-terminal His$_6$-tag. The resulting constructs were used to transform *Escherichia coli* BL21 (DE3). The plasmid encoding for H454S hAIF$_{\Delta 1-102}$ was obtained by site-directed mutagenesis at Mutagenex and similarly cloned. Expression and purification of the mutants were performed following the procedures described for the wild-type (WT) protein.[14] For the K177W, E314S, and K177W/E314S variants, 1 mL of 2 mM FAD solution was added during the incubation of the lysate with the resin.

Molecular Weight Determination by Size Exclusion Chromatography. hAIF$_{\Delta 1-102}$ variants (90 μM), either in the presence or absence of a 10-fold excess of NADH, were loaded onto a HiPrep 26/60 SephacrylS-200 high resolution (GE Healthcare) column attached to a fast pressure liquid chromatographic system (GE Healthcare), in 50 mM Tris-HCl, pH 8.0, 150 mM NaCl, at a flow rate of 0.5 mL/min. The column was calibrated with a LMW calibration kit (6 proteins in the 6400−160000 Da range).

Stabilization of Cross-Linked Oligomers and Electrophoretic Analysis. Reaction mixtures containing 3 μM of the different hAIF$_{\Delta 1-102}$ mutants in 10 mM phosphate, pH 8.0, and a 100-fold excess of the homobifunctional-bis-[sulfosuccinimidyl]-suberate (BS^3) (Pierce) cross-linker were incubated for 30 min at room temperature either in the absence or in the presence of 300 μM NADH. Reactions were terminated by addition of the denaturing bromophenol blue sample buffer. Samples were resolved by 12% SDS-PAGE.

Atomic Force Microscopy Imaging. Protein solutions (0.5 μM) in PBS, pH 7.0, were incubated on exfoliated mica sheets (Electron Microscopy Sciences) for 10 min and washed with the same buffer to achieve immobilization. Proteins were also incubated with 100 μM NADH at 4 °C under mild stirring and pretreated with 100 μM of BS^3 for 50 min at 25 °C. Atomic force microscopy (AFM) measurements were performed in a Cervantes Fullmode AFM (Nanotec Electrónica S.L.) using the Jumping Mode with silicon nitride microlevers (MSNL; Bruker Probes) under low applied forces[17] as described.[14] Twenty different areas of 500 nm^2 from four samples per assayed condition were analyzed. Percentages of each species were estimated as the existing number of this species with respect to the total number in the sample. The associated error was calculated from the dispersion of results in the analysis of different images corresponding to the different areas.

Spectroscopic Measurements. Spectroscopic and steady-state analysis were carried out in a Cary 100 Bio spectrophotometer (Varian). Concentrations were determined using the molar absorbance of the mutants previously estimated at the band I of the flavin (~450 nm) upon release of FAD by incubation with 3 M guanidinium chloride or by boiling at 90 °C for 5 min. The calculated extinction coefficient values were 14.65, 14.38, and 15.26 mM^{-1} cm^{-1} for F310G, P173G, and H454S at the maximum for the band I of the flavin in each species. Steady-state activities were measured in air saturated 50 mM potassium phosphate, pH 8.0, using NAD(P)H as the substrate donor and either 95 μM dichlorophenolindophenol (DCPIP) or 0.375 mg/mL cytochrome *c* (Cytc) as acceptors.[14] Processes were followed at the wavelengths of maximal molar differential extinction coefficient for DCPIP and Cytc upon reduction ($\Delta\varepsilon_{620nm}$ = 21 mM^{-1} cm^{-1} and $\Delta\varepsilon_{550nm}$ = 20 mM^{-1} cm^{-1} respectively[14,18]). Parameters were determined by fitting initial reaction rates at different NAD(P)H concentrations to the Michaelis−Menten equation for one substrate, $v/e = k_{cat}[S]/(K_m + [S])$, where e represents the enzyme concentration, K_m the Michaelis constant, and k_{cat} the maximal turnover number of the enzyme. The catalytic efficiency, k_{cat}/K_m, was determined by fitting initial rate data to the normalized Michaelis−Menten equation $v/e = (k_{cat}/K_m)[S]/(1+((k_{cat}/\{K_m)[S]/k_{cat}\}))$.

Transient Kinetics Measurements. Stopped-flow measurements were carried out under anaerobic conditions in a SX17.MV spectrometer (Appl. Phot. Ltd.) using a photodiode array detector and the Xscan software as previously reported.[14] Briefly, tonometers containing enzyme or substrate solutions were made anaerobic by successive evacuation and flushing with argon. Drive syringes in the apparatus were made anaerobic by sequentially passing dithionite and O_2-free buffer solutions before introducing the reagents. Measures were carried out in 50 mM potassium phosphate, pH 8.0, at 24 °C

DOI: 10.1021/acs.biochem.5b00696
Biochemistry 2015, 54, 5175−5184

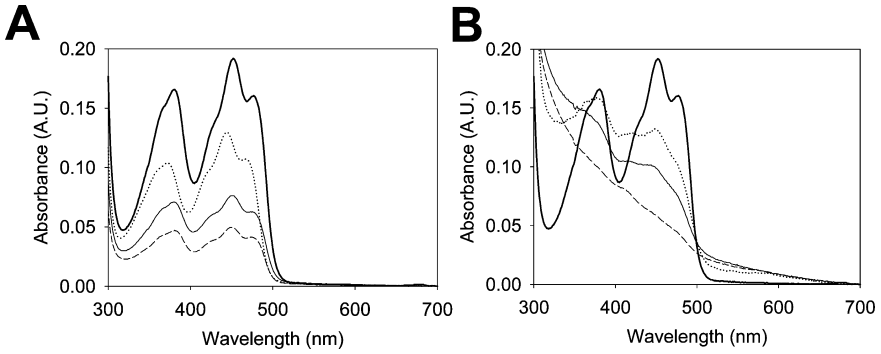

Figure 2. Visible absorption spectra of purified hAIF$_{\Delta 1-102}$ variants. (A) Spectra of WT (13.9 μM, solid line), P173G (9.0 μM, dotted line), F310G (5.2 μM, thin solid line), and H454S (3.3 μM, dashed line) hAIF$_{\Delta 1-102}$. (B) Spectra of WT (solid line), E314S (dotted line), K177W/E314S (thin solid line), and K177W (dashed line) hAIF$_{\Delta 1-102}$. Spectra were recorded in 50 mM potassium phosphate, pH 8.0, at 24 °C. Different protein concentrations were used for each variant to clarify the figure.

with ~10 μM of the P177G, F310G, and H454S hAIF$_{\Delta 1-102}$ variants and a range of NADH concentrations (0.03−10 mM). The enzyme and NADH concentrations are the final ones obtained after mixing equal volumes of substrate and enzyme. The observed rates for the HT event (k_{obs}) were calculated by global analysis and numerical integration methods (simultaneously using all spectral data in the 400−800 nm region along time evolution) by fitting to a single step model (A → B). When a saturation profile on the pyridine nucleotide concentration was observed, k_{obs} values were fit to the $k_{obs} = k_{HT}S/(K_d + S)$ equation describing formation of an enzyme:substrate complex prior to the HT process, where k_{HT} is the limiting rate constant for HT from the pyridine nucleotide coenzyme to the FAD cofactor of hAIF, and K_d is the hAIF:coenzyme dissociation constant.

Data Analysis. Data were fitted and shown in figures using SigmaPlot (Systat. Software Inc. Richmond, CA, USA) and Pro-K (Applied Photophysics Ltd.). Structural figures were prepared using Pymol.[19]

Sequences. The amino acid sequences used to create sequence logo were downloaded from GenBank of NCBI: AIF from *Callithrix jacchus* (JAB49837.1), *Acromyrmex echinatior* (EGI60694.1), *Camponotus floridanus* (EFN62354.1), *Fopius arisanus* (JAG73209.1), *Drosophila melanogaster* (NP_001259907), *Mus musculus* (AAH03292.1), *Rattus norvegicus* (AAH72697.1), *Cricetulus griseus* (ERE65754.1), *Heterocephalus glaber* (EHB03571.1), *Fukomys damarensis* (KFO21949.1), *Homo sapiens* (AAD16436.1), *Pan troglodytes* (JAA39924.1), *Macaca fascicularis* (EHH61217.1), *M. mulatta* (EHH31073.1), *Myotis brandtii* (EPQ11765.1), *Pteropus alecto* (ELK12150.1), *Bos taurus* (NP_001179913.1), *Gallus gallus* (NP_001007491.1), *Chelonia mydas* (EMP32088.1), *Crotalus adamanteus* (JAI14305.1), *Danio rerio* (NP_956396.2), *Larimichthys crocea* (KKF32773.1), *Trichuris trichiura* (CDW51950.1), *Culex quinquefasciatus* (EDS38062), *Anopheles darlingi* (ETN64791.1), *Cassostrea gigas* (EKC36189.1), *Toxocara canis* (KHN78197.1), WAH-1 from *Caenorhabditis elegans* (NP_001263729.1), FR from *Pseudomonas sp. KKS102* (Q52437), AMID from *H. sapiens* (Q9BRQ8.1), BphA4 from *Pseudomonas sp. UW4* (AFY17347.1), MDAR from *Cucumis sativus* (BAA05408.1), MDAR (NADH) from *Arabidopsis thaliana* (AEE74839.1), and MDAR from *A. thaliana* (BAA12349.2).

RESULTS

Spectroscopic Properties of the hAIF$_{\Delta 1-102ox}$ Variants. The single P173G, K177W, F310G, E314S, and H454S hAIF$_{\Delta 1-102}$ and the double K177W/E314S hAIF$_{\Delta 1-102}$ variants were purified to homogeneity as described previously for the WT protein.[14] Very similar UV−visible absorption spectra were observed for F310G, H454S, and WT hAIF$_{\Delta 1-102}$, showing an A_{280}/A_{451} ratio ≈ 11 (Figure 2A). The spectra exhibited the typical bands I and II of the flavin at 451 and 380 nm, respectively, and a shoulder at 467 nm, indicating that the flavin cofactor was in the oxidized state and correctly incorporated into the protein. Therefore, these mutations compromised neither protein folding nor interaction with the FAD cofactor. In contrast, the P173G variant shifted the maxima to 444 and 372 nm, as well as the shoulder to 461 nm, revealing differences in the flavin environment compared with WT hAIF$_{\Delta 1-102ox}$ (Figure 2A). This may be due to a diminution of the rigidity imposed by the proline in the loop containing it. Finally, visible spectra for the K177W, E314S, and K177W/E314S variants showed distorted shapes for the band-I and band-II of the flavin, large A_{280}/A_{451} ratios (~18, ~20, and ~16, respectively), and slight turbidity. These mutants despite being yellow easily precipitated during purification and manipulation. These observations indicate that replacements of Lys177 by tryptophan and of Glu314 by serine produce deleterious effects on FAD stability into the active site of hAIF$_{\Delta 1-102}$ (Figure 2B), producing variants almost depleted of the flavin cofactor. Due to the low purification yield and capacity to retain the FAD cofactor in these mutants, further studies were restricted to P173G, F310G, and H454S hAIF$_{\Delta 1-102}$.

Quaternary Assemblies of the hAIF$_{\Delta 1-102}$ Variants. As reported for the WT, gel filtration chromatography was initially used to characterize the effects of the P173G, F310G, and H454S mutations on the hAIF$_{\Delta 1-102}$ monomer/dimer transition upon incubation with NADH.[14] All the hAIF$_{\Delta 1-102ox}$ variants eluted as a single peak with apparent molecular weights (MW) corresponding to the monomeric forms, similarly to the WT (Data not shown). In contrast to the WT enzyme, the P173G and F310G variants remained eluting as a monomeric peak upon incubation with NADH, while the H454S mutant eluted as a broad peak. The averaged MW estimated for the H454S mutant broad peak was ~1.4-times higher than that of the monomeric protein, while the dimer reported for the WT corresponded to an apparent MW ≈ 2.3−2.7-times higher than the monomeric protein.[14] This behavior might be indicative of

DOI: 10.1021/acs.biochem.5b00696
Biochemistry 2015, 54, 5175−5184

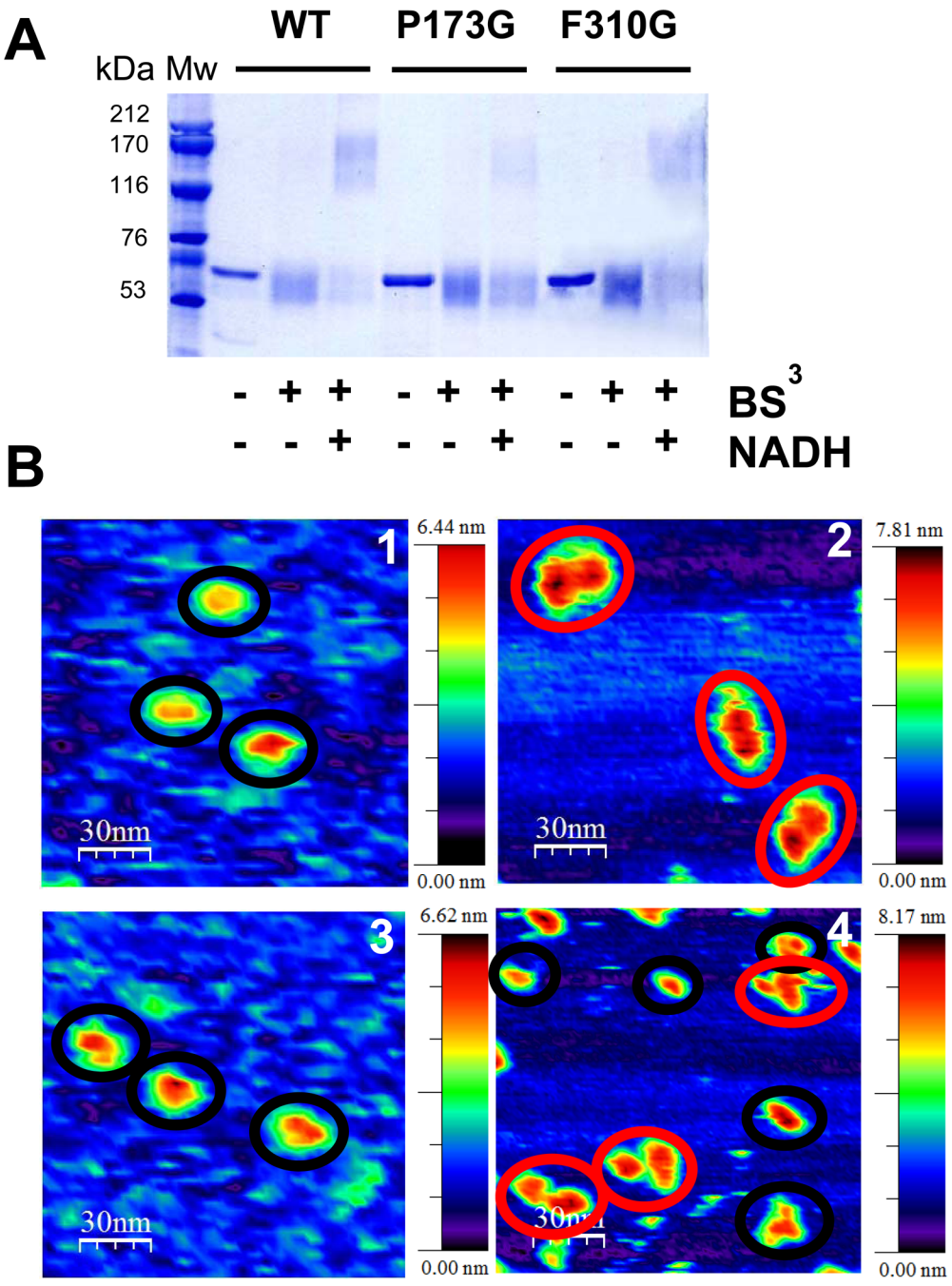

Figure 3. Evaluation of $hAIF_{\Delta 1-102}$ dimerization. (A) SDS-PAGE patterns of WT, P173G, and F310G $hAIF_{\Delta 1-102}$ upon incubation with BS^3 and NADH. (B) Jumping mode AFM topography representative images of (1) F310G $hAIF_{\Delta 1-102ox}$, (2) F310G $hAIF_{\Delta 1-102}$ incubated with NADH and BS^3, (3) H454S $hAIF_{\Delta 1-102ox}$, and (4) H454S $hAIF_{\Delta 1-102}$ incubated with NADH and BS^3. Monomers and dimers are highlighted with black and red circles, respectively. Images were obtained in PBS, pH 7.0. The area of the images corresponds to 150 nm^2. Images in panels 1−3 were the originally scanned, while panel 4 is a zoomed image of an original scan of a 500 nm^2 area.

dimer dissociation along the chromatographic process. To check such a possibility, further studies were carried out in the presence of the BS^3 cross-linker to stabilize the presumptive formation of dimers upon reaction with NADH.[12,14] After incubation of P173G, F310G, and H454S $hAIF_{\Delta 1-102ox}$ with a 100-fold excess of BS^3, only a monomer of ∼55 kDa was assessed by SDS-PAGE, similarly to the WT (Figure 3A). However, when the $hAIF_{\Delta 1-102}$ mutants were incubated with both BS^3 and NADH, a broad band covering the 130−170 kDa Mw range appeared, as also reported for the WT (Figure 3A).[14] This indicates that these mutants are also able to dimerize upon interaction with NADH.

AFM was also used to analyze at the single molecule level the quaternary organization of the F310G and H454S variants in both oxidized and NADH-reduced states (Figure 3B). AFM imaging of the $hAIF_{\Delta 1-102ox}$ mutants revealed a homogeneous distribution of isolated molecules of diameter 6.5 ± 0.5 nm immobilized on the mica surface, identified as monomers (Figure 3B, panels 1 and 3), similarly to the WT enzyme (See Figure 1B in Ferreira et al).[14] After treatment with NADH both in the presence (Figure 3B, panels 2 and 4) and absence of BS^3

DOI: 10.1021/acs.biochem.5b00696
Biochemistry 2015, 54, 5175−5184

Table 1. Steady-State Kinetics Parameters for the Reactions of hAIF$_{\Delta 1\text{-}102}$ Variants as Reductases[a]

hAIF$_{\Delta 1-102}$ variant	electron acceptor	NADH as electron donor			NADPH as electron donor			specificity
		k_{cat} (s^{-1})	K_m^{NADH} (μM)	k_{cat}/K_m^{NADH} (s^{-1} mM^{-1})	k_{cat} (s^{-1})	K_m^{NADPH} (μM)	k_{cat}/K_m^{NADPH} (s^{-1} mM^{-1})	$[k_{cat}/K_m^{NADH}]/[k_{cat}/K_m^{NADPH}]$
WT[b]	DCPIP	1.5 ± 0.1	273 ± 31	5.6 ± 1.6	0.04 ± 0.005	896 ± 31	0.06 ± 0.02	93.3 ± 40.9
	Cytc	1.3 ± 0.4	203 ± 75	6.4 ± 1.7				
P173G	DCPIP	3.2 ± 0.1	312 ± 111	11.8 ± 2.1	[c]	[c]	[c]	[c]
	Cytc	2.6 ± 0.2	163 ± 39	19.8 ± 4.02				
F310G	DCPIP	4.2 ± 0.2	75 ± 19	53.1 ± 8.5	3.0 ± 0.2	777 ± 179	5.4 ± 0.6	9.8 ± 1.9
	Cytc	1.2 ± 0.1	19 ± 2	56.0 ± 7.4				
H454S	DCPIP	1.6 ± 0.1	224 ± 70	7.6 ± 1.6	[c]	[c]	[c]	[c]
	Cytc	0.4 ± 0.02	174 ± 37	2.8 ± 0.3				

[a]Assays performed in 50 mM potassium phosphate buffer, pH 8.0, at 24 °C. [b]Data from ref 14. [c]Reaction was not detected.

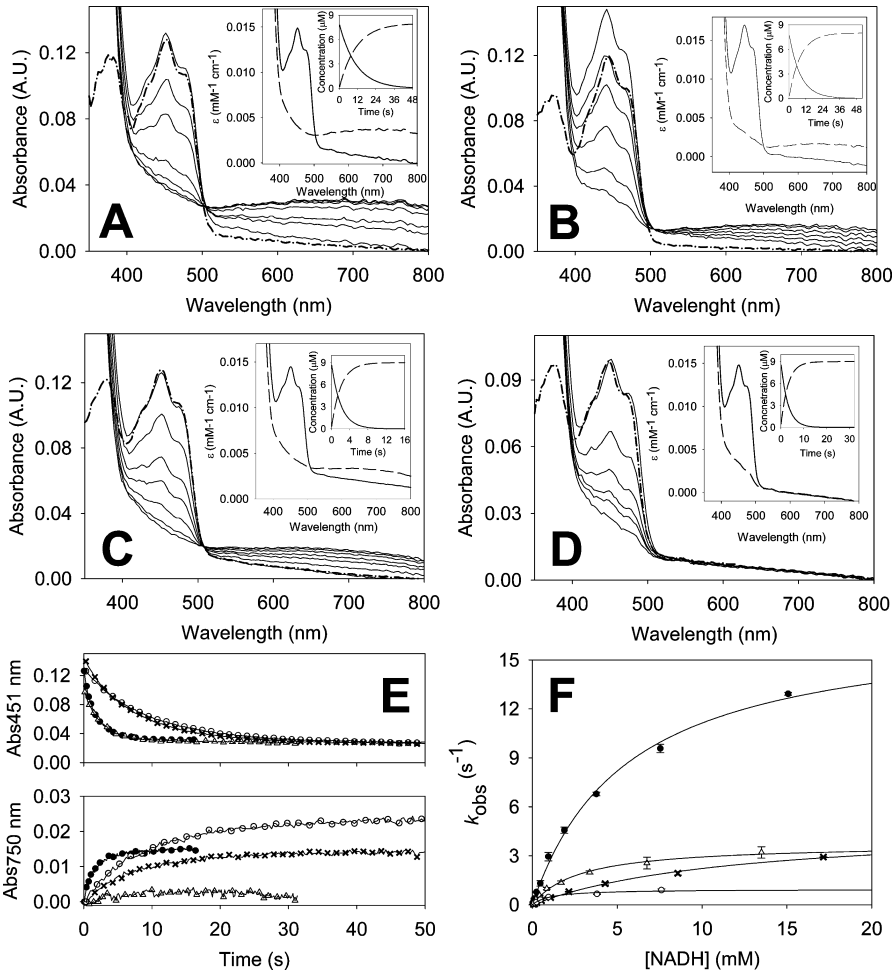

Figure 4. Transient kinetics for the HT processes from NADH to the hAIF$_{\Delta 1-102}$ variants. The reaction of hAIF$_{\Delta 1-102ox}$ WT and their variants (~8, 7, 9, and 6 μM for WT, P173G, F310G, and H454S, respectively) with NADH (475 μM for WT and 312 μM for mutants) was followed in a stopped-flow spectrophotometer in 50 mM potassium phosphate, pH 8.0, at 24 °C under anaerobic conditions. Spectra recorded at different times after mixing are shown for (A) WT after 0.3, 3.6, 6.9, 16.7, 26.5, 36.4, and 46 s, (B) P173G after 0.33, 1.97, 3.60, 6.88, 13.43, 21.63, and 52.76 s, (C) F310G after 0.08, 0.49, 1.31, 2.13, 3.77, 7.04, and 13.19 s, and (D) H454S after 0.16, 0.98, 1.8, 3.45, 5.00, 6.71, and 31.29 s. In all cases, the hAIF$_{\Delta 1-102ox}$ spectrum before mixing is shown as a dashed line. The corresponding insets show the deconvolution of the spectral changes during HT reactions fitting to a one step model (A→B) and the evolution of these species over time (A and B are spectral species reflecting distribution of reactants and products respectively). (E) Comparison of the kinetics traces at 451 and 750 nm during protein reduction (upper panel) and CTC formation (lower panel) for WT (○), P173G (×), F310G (●), and H454S (△). For clarity, in the lower panel all traces have been normalized starting at absorbance zero. (F) Dependence of the observed rate constants for the HT from NADH to WT (○), P173G (×), F310G (●), and H454S (△) hAIF$_{\Delta 1-102}$ versus the coenzyme concentration.

(not shown), the assayed mutants appeared also as dimers. The attribution of the dimeric character from the isolated particles was unequivocally found by performing topographic profiles with the zoom and profile functions of the WSxM software[20] with subnanometer resolution in the Z axis. F310G hAIF$_{\Delta 1-102}$ dimerized up to 65% ± 5% of the total protein in the sample

DOI: 10.1021/acs.biochem.5b00696
Biochemistry 2015, 54, 5175−5184

with BS^3 (Figure 3B, panel 2) and up to 15% ± 5% in its absence, while the other variant produced a similar proportion of dimers in both conditions (25% ± 5%).

Therefore, results obtained in the presence of BS^3 confirmed that the mutations introduced at P173, F310, and H454 do not prevent formation of $hAIF_{\Delta 1-102}$ dimers upon interaction with NADH. Moreover, the lack of observation of such dimers in the absence of the cross-linker in exclusion chromatography suggests that the mutations have a negative impact on the strength of the interaction between protomers within the dimer. As will be described below, such a decrease in dimer stabilization will also relate to a lower stabilization of CTC in these variants.

Efficiency of $hAIF_{\Delta 1-102}$ Mutants as NAD(P)H Dependent Reductases. The efficiency of the different $hAIF_{\Delta 1-102}$ mutants to oxidize NADH was evaluated under steady-state conditions using typical electron acceptors already proved for their ability to exchange electrons with the WT enzyme (Table 1): DCPIP and Cytc.[14] The H454S variant turnover with DCPIP was similar to that of the WT enzyme (1.6 ± 0.1 s^{-1}), while the P173G and F310G mutations caused a modest increase in k_{cat} (2- and 3-fold, respectively). When using Cytc as acceptor, the turnover rate for F310G was in the same range as that reported for the WT protein (~1.3 s^{-1}), whereas the rate increased and decreased for P173G (k_{cat} within ~2-fold increase) and H454S (k_{cat} within ~3-fold decrease), respectively. K_m^{NADH} values for the P173G and H454S variants were similar to that for the WT, independent of the acceptor used, while the F310G variant showed a considerable increase (4- and 10-fold when using DCPIP and Cytc, respectively). None of the variants showed the ability to efficiently be oxidized by molecular oxygen upon NADH reduction, so they have no NADH oxidase activity.

The ability of the different $hAIF_{\Delta 1-102}$ variants as reductases was also evaluated by using NADPH as electron donor and DCPIP as acceptor. Under such conditions, WT $hAIF_{\Delta 1-102}$ is considerably less efficient than when NADH is used; k_{cat} and K_m^{NADPH} values are 37-fold lower and 3-fold higher (Table 1), respectively.[14] No activity was detected for P173G and H454S mutants when NADPH was used as a reductant. In contrast, the F310G variant exhibited a strong increase in turnover (75-fold) compared with the WT (Table 1). Overall, the k_{cat} and K_m values determined for F310G $hAIF_{\Delta 1-102}$ indicate that this mutation reduces the specificity for NADH versus NADPH when compared with the WT protein.

Efficiency of $hAIF_{\Delta 1-102}$ Mutants As Hydride Acceptors from NADH. We also used stopped-flow transient kinetics to analyze the effects of the mutations on the NADH dissociation constant for the NADH:$hAIF_{\Delta 1-102}$ complex, K_d^{NADH}, as well as on the HT rate constant, k_{HT}, from the nicotinamide ring of NADH to the isoalloxazine ring of $hAIF_{\Delta 1-102}$. Contrary to what was observed for the WT, the NADH reduced P173G, F310G, and H454S mutants were sensitive to reoxidization by molecular oxygen. Therefore, assays for the mutants were conducted under anaerobic conditions. Spectral evolution upon mixing the P173G, F310G, and H454S variants with NADH showed a decrease in the absorbance at 451 nm consistent with full reduction of the FAD cofactor (Figure 4A–D). HT from NADH to FAD in the P173G and F310G mutants, as well as in the WT enzyme, was accompanied by the progressive formation of a long-wavelength broad band related to the formation of isoalloxazine:NAD^+ CTCs (Figure 4B,C).[14] Nevertheless, the intensity of the CTC bands (band area in the 510–800 nm minus that of the free protein) for the P173G and F310G variants was ~24% and ~12% lower, respectively, than what was observed for the WT enzyme (Figure 4B,C versus Figure 4A,E). In contrast, FAD reduction in the H454S variant took place without the spectroscopic detection of any CTC (Figure 4D,E). This indicates either a considerable reduction of the amount of CTC stabilization or the production of CTCs with different charge distribution between the reacting rings. The lower or absence of CTC stabilization in the mutants indicates that substrate accommodation is modulated by these active-site mutations, as supported below for the calculated K_d^{NADH} values (see Figure 4F and Table 2). Global analysis of the reaction spectral time courses fit to a one step model (A → B) for the three mutants (insets of Figure 4A,B,C,D). As reported for the WT enzyme,[14] the observed reactions were attributed to formation of the NADH:$hAIF_{\Delta 1-102}$ complex and HT from the nicotinamide of the coenzyme to the isoalloxazine ring of FAD to stabilize the reduced enzyme:NAD^+ complex.

Table 2. Pre-Steady-State Kinetics Parameters for the Anaerobic Reduction of the $hAIF_{\Delta 1-102}$ Variants by NADH[a]

	k_{HT} (s^{-1})	K_d^{NADH} (μM)	k_{HT}/K_d^{NADH} (s^{-1} mM^{-1})
WT[b]	1.0 ± 0.1	1055 ± 302	0.95 ± 0.19
P173G	4.9 ± 0.3	12060 ± 1289	0.41 ± 0.05
F310G	17.3 ± 0.7	5585 ± 499	3.10 ± 0.30
H454S	3.7 ± 0.2	2743 ± 295	1.35 ± 0.16

[a]Assays were performed in 50 mM potassium phosphate buffer, pH 8.0, at 24 °C. [b]Data from ref 14.

k_{obs} for the HT event exhibited a hyperbolic dependence on NADH concentration (Figure 4F) that allowed k_{HT} and K_d^{NADH} determination (Table 2) upon fitting to the equation $k_{obs} = k_{HT}S/(K_d + S)$, which describes an essentially irreversible reaction. The k_{HT} values for the P173G, F310G, and H454S variants indicated processes ~5-, ~17- and ~4-fold faster, respectively, than that of the WT enzyme, suggesting that HT event by itself is favored by the mutations. On the other hand, a decrease in the affinity for the pyridine nucleotide was produced, with K_d^{NADH} values 12-, 5-, and 3-fold higher for P173G, F310G, and H454S variants, respectively, than for WT. These changes make the P173G variant slightly less efficient than the WT in the HT event, while the other two mutants are slightly more efficient (up to ~3-fold for F310G).

DISCUSSION

Here we have carried out a mutational analysis on several structurally relevant and highly conserved residues at the environment of the hAIF isoalloxazine and the $NAD(H)_A$ nicotinamide rings to further depict the role of this coenzyme binding site in the enzyme NADH-reductase activity. K177 and E314 are highly conserved in sequences of AIF and related enzymes from different species (Figure 1B), as well as in AIF and BphA4 structures.[15,16] Our results indicate that mutations at these positions critically affect incorporation of the FAD cofactor in the hAIF active site, as shown for mAIF and BphA4.[7,16] In $hAIF_{ox}$, $mAIF_{ox}$, and $BphA4_{ox}$ the side chains of these lysine and glutamate residues are stabilized by mutual interaction, with the lysine salt-bridging the glutamate side chain and forming bifurcated H-bonds with the N5 and O4 atoms of FAD.[7,15,16] HT from the nicotinamide of NADH to N5 of FAD induces a redox-dependent conformational

DOI: 10.1021/acs.biochem.5b00696
Biochemistry 2015, 54, 5175–5184

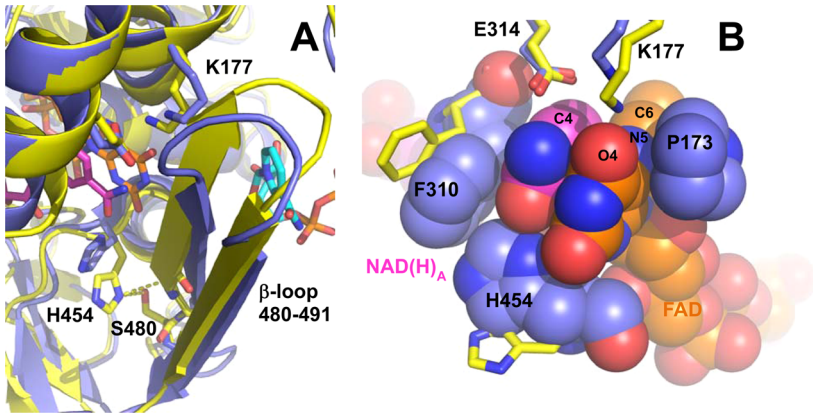

Figure 5. Detail of conformational changes observed upon hAIF reduction. (A) Structural displacement in the 480−491 region and displacement of K177 and H454 (pdb 4BV6). (B) Stacking organization at the FAD isoalloxazine and the nicotinamide rings of $NAD(H)_A$ in the $hAIF_{\Delta 1-102rd}$:2NAD(H) complex (pdb 4BUR). Side chains of P173, F310, and H454 are shown as balls for $hAIF_{\Delta 1-102rd}$:2NAD(H) and as sticks for $hAIF_{\Delta 1-121ox}$. Color codes for image features as in Figure 1A.

displacement of K177 that breaks these bifurcated H-bonds. As a consequence, the 480−491 β-loop (Figures 1A and 5A) at the C-terminal domain shifts backward contributing to the displacement of H454 at the NADH-binding domain and to the stabilization of the $NAD(H)_A$ nicotinamide. Such displacement of the 480−491 β-loop additionally allows stacking of $NAD(H)_B$ at its back site. Thus, replacements at E314 and K177 in $hAIF_{\Delta 1-121ox}$ might modify the active site structural conformation as well as the arrangements suffered upon NADH reduction, as suggested for mAIF variants.[7] Replacement of E314 by the noncharged and shorter serine would modify the K177 conformation regarding both the isoalloxazine and the 480−491 β-loop. Substitution of K177 by a tryptophan will alter interactions with E314 and the isoalloxazine. However, the major effects of the K177W mutation would relate to the aromatic character and larger volume of the introduced tryptophan side chain, surely inducing displacement of E314, of the isoalloxazine ring, and of the 480−491 β-loop. The double mutant, K177W/E314S, was expected to compensate changes in volume, but its spectroscopic properties also indicated low FAD incorporation. Therefore, the low capability of these mutants to incorporate FAD prevented their further characterization.

The P173 residue of hAIF is highly conserved and generally followed by another proline residue in oxygenase-coupled NADH-dependent ferredoxin reductases (Figure 1B). In AIF and BphA4, these tandem proline residues constitute the N-terminus of a short α-helix, with P173 interacting by van der Waals contacts with the *si*-face of the isoalloxazine ring (Figure 5B). Thus, P173 seems to be essential to place this ring, as well as to stack it against the nicotinamide moiety of $NAD(H)_A$ in the CTC structure (Figures 1A and 5B).[14,15] Although removal of the proline side-chain in P173G $hAIF_{\Delta 1-102}$ slightly alters the electronic properties of the flavin compared with the WT (Figure 2), as expected from the close proline−flavin stacking, k_{cat} and k_{HT} remain in the WT range (Tables 1 and 2). This indicates that the HT is the rate-limiting step in P173G hAIF catalysis, similarly to the WT. Moreover, replacement of P173 decreases the affinity for NADH, the stability of the protein dimer, and the $hAIF_{\Delta 1-102\ rd}$:2NAD(H) CTC stabilization, while it increases the CTC reactivity with molecular oxygen (Table 2 and Figure 4). These parameters, NADH affinity and CTC and dimer stability, are closely related and, as previously reported for the WT enzyme,[14] suggest that the role of P173 in setting the position and the properties of the isoalloxazine ring in hAIF is key for NADH binding and CTC stabilization.

The F310G and H454S mutations have low impact on FAD incorporation into the hAIF active site (Figure 2A). Regarding their steady-state behavior, the more relevant effects are a decrease in K_m^{NADH} and a considerable specificity decrease for NADH versus NADPH for the F310G variant. When analyzed under pre-steady-state conditions, both mutants, but particularly F310G, have faster k_{HT} than the WT. The significant differences between k_{HT} and k_{cat} values for the F310G variant suggest that, in this mutant, the reductive half-reaction is not the rate-limiting step in catalysis. Major impacts of these mutations relate to the lower stabilization of dimers and CTCs upon NADH reduction (Figure 4) and to the faster reactivity of their NADH reduced states with molecular oxygen, when compared with the WT. These effects are consistent with a decrease in the affinity for NAD^+ in the reduced variants. This observation indicates that both residues, but particularly H454, play a key role in stabilizing the $hAIF_{\Delta 1-102\ rd}$:2NAD(H) CTC intermediate and that their mutation might facilitate the access of molecular oxygen to the reduced active site. These results agree with the very compact architecture of the $hAIF_{\Delta 1-102\ rd}$:2NAD(H) active site,[14] where the position of the nicotinamide of $NAD(H)_A$ is determined by interactions with side chains of E314, F310, and H454 (Figures 1A and 5B). F310 and H454 are highly conserved in AIF species but show replacements in related enzymes (Figure 1B). In BphA4, they match with a valine and a threonine, respectively. The valine substitution stacks the nicotinamide toward the isoalloxazine but only covers the central portion of the ring. Similarly to H454 in hAIF, the corresponding threonine in BphA4 is at the N-terminus of an α-helix. The positive partial charge of this α-helix stabilizes the negative charge of the reduced isoalloxazine ring. However, the side chain of this threonine points in the opposite direction, to the nicotinamide and isoalloxazine rings, while a water molecule occupies what was the H454 position in AIF. Thus, when in complex with the pyridine nucleotide, BphA4 shows a considerably less compact active site than AIF, suggesting solvent molecules have an easier access to it.[7] This difference has to be related to the very low efficiency of the HT process from NADH to AIF in comparison with other members of the family: hAIF shows turnovers, k_{HT}, and K_m^{NADH}

DOI: 10.1021/acs.biochem.5b00696
Biochemistry 2015, 54, 5175−5184

values in the 1−6 s^{-1}, 1 s^{-1}, and 0.3−1 mM ranges, respectively, while the corresponding parameters for related flavoenzymes indicate that they are much more efficient reductases. Thus, turnovers and k_{HT} values in the range of 150 s^{-1} and 526 s^{-1}, respectively, have been reported for BphA4,[16] whereas for MDAR turnovers and K_m^{NADH} oscillate in the 100−130 s^{-1} and 4−12 μM ranges, respectively.[21,22] Another remarkable difference is the rate-limiting step; the oxidative half-reaction for BphA4 and MDAR catalysis and the reductive half-reaction for AIF.

In conclusion, these results indicate that the P173, K177, and E314 residues have key roles in FAD binding, creating a particular environment required for the hAIF NADH-dependent functions. Additionally, the conservation of these residues in other family members suggests the existence of a general motif for FAD binding. In contrast, the F310 and H454 residues contribute to $NADH_A$ binding and NAD^+_A stabilization in the hAIF active site after the HT to the flavin. The fact that these residues are not conserved in other members of the family, where less compact active sites are found in the coenzyme-bound state, indicates that they strongly contribute to the CTC stabilization and to the low efficiency of AIF as a reductase. This low efficiency of AIF when accepting a hydride from NADH appears key in redox metabolism of healthy cells, since mutations altering it have been related to several mitochondrial human disorders causing progressive mitochondrial encephalomyopathy.[23−26]

AUTHOR INFORMATION

Corresponding Authors

*Milagros Medina. Mailing address: Departamento de Bioquímica y Biología Molecular y Celular, Facultad de Ciencias, Universidad de Zaragoza, Pedro Cerbuna, 12, 50009 Zaragoza, Spain. Tel: +34976762476. Fax: +34976762123. E-mail: mmedina@unizar.es.

*Patricia Ferreira. Mailing address: Departamento de Bioquímica y Biología Molecular y Celular, Facultad de Ciencias, Universidad de Zaragoza, Pedro Cerbuna, 12, 50009 Zaragoza, Spain. Tel: +34876553774. Fax: +34976762123. E-mail: ferreira@unizar.es.

Author Contributions

R.V. carried out the biochemical and biophysical characterizations, produced figures, interpreted the results, and contributed to write the paper, M.D.M., S.A.S., and M.L.P. designed and constructed the mutations, cloned them into the pET28a expression vector, and performed some preliminary characterizations, C.M. and A.L. carried out the AFM studies, A.U. produced some mutants and did some preliminary characterizations, P.F. contributed to design the study, carried out the biochemical and biophysical characterizations, produced figures, interpreted the results, and wrote the paper, and M.M. conceived the study, interpreted the results, produced the structural figures, and wrote the paper.

Funding

This work has been supported by the Spanish Ministry of Economy and Competitiveness (Grant BIO2013-42978-P to M.M.) and by D.G.A.-FEDER BE-18. A.L. thanks Fundación ARAID. R.V. and C.M. thank MICINN and DGA, respectively, for Ph.D. fellowships.

Notes

The authors declare no competing financial interest.

ACKNOWLEDGMENTS

The authors thank I. Echániz and J.L. Diez-Ferrer for technical assistance.

ABBREVIATIONS

AIF, Apoptosis Inducing Factor; mAIF, murine isoform of AIF; hAIF, human isoform of AIF; $hAIF_{\Delta 1-102}$, human isoform of AIF after deletion of the first N-terminal 102 residues; $hAIF_{\Delta 1-102ox}$, oxidized $hAIF_{\Delta 1-102}$; $hAIF_{\Delta 1-102rd}$, reduced $hAIF_{\Delta 1-102}$; AMID, human apoptosis inducing factor-like mitochondrion associated inducer of death; WAH-1, AIF homologue from *C. elegans*; MDAR, monodehydroascorbate reductase from *A. thaliana* chloroplasts; BphA4, biphenyl 2,3-dioxygenase ferredoxin reductase subunit from *R. palustris*; FR , ferredoxin reductase; FAD or FAD_{ox}, oxidized form of the flavin adenine nucleotide; $FADH_2$ or FAD_{red}, two-electron reduced form of the flavin adenine nucleotide; DCPIP, 2,6-dichlorophenolindophenol; CTC, charge transfer complex; AFM, atomic force microscopy; Cytc, cytochrome *c*; BS^3, homobifunctional-bis[sulfosuccinimidyl]-suberate; HT, hydride transfer; WT, wild-type

REFERENCES

(1) Klein, J. A., Longo-Guess, C. M., Rossmann, M. P., Seburn, K. L., Hurd, R. E., Frankel, W. N., Bronson, R. T., and Ackerman, S. L. (2002) The harlequin mouse mutation downregulates apoptosis-inducing factor. *Nature 419*, 367−374.

(2) Vahsen, N., Cande, C., Briere, J. J., Benit, P., Joza, N., Larochette, N., Mastroberardino, P. G., Pequignot, M. O., Casares, N., Lazar, V., Feraud, O., Debili, N., Wissing, S., Engelhardt, S., Madeo, F., Piacentini, M., Penninger, J. M., Schagger, H., Rustin, P., and Kroemer, G. (2004) AIF deficiency compromises oxidative phosphorylation. *EMBO J. 23*, 4679−4689.

(3) Cande, C., Vahsen, N., Kouranti, I., Schmitt, E., Daugas, E., Spahr, C., Luban, J., Kroemer, R. T., Giordanetto, F., Garrido, C., Penninger, J. M., and Kroemer, G. (2004) AIF and cyclophilin A cooperate in apoptosis-associated chromatinolysis. *Oncogene 23*, 1514−1521.

(4) Urbano, A., Lakshmanan, U., Choo, P. H., Kwan, J. C., Ng, P. Y., Guo, K., Dhakshinamoorthy, S., and Porter, A. (2005) AIF suppresses chemical stress-induced apoptosis and maintains the transformed state of tumor cells. *EMBO J. 24*, 2815−2826.

(5) Susin, S. A., Lorenzo, H. K., Zamzami, N., Marzo, I., Snow, B. E., Brothers, G. M., Mangion, J., Jacotot, E., Costantini, P., Loeffler, M., Larochette, N., Goodlett, D. R., Aebersold, R., Siderovski, D. P., Penninger, J. M., and Kroemer, G. (1999) Molecular characterization of mitochondrial apoptosis-inducing factor. *Nature 397*, 441−446.

(6) Ye, H., Cande, C., Stephanou, N. C., Jiang, S., Gurbuxani, S., Larochette, N., Daugas, E., Garrido, C., Kroemer, G., and Wu, H. (2002) DNA binding is required for the apoptogenic action of apoptosis inducing factor. *Nat. Struct. Biol. 9*, 680−684.

(7) Mate, M. J., Ortiz-Lombardia, M., Boitel, B., Haouz, A., Tello, D., Susin, S. A., Penninger, J., Kroemer, G., and Alzari, P. M. (2002) The crystal structure of the mouse apoptosis-inducing factor AIF. *Nat. Struct. Biol. 9*, 442−446.

(8) Miramar, M. D., Costantini, P., Ravagnan, L., Saraiva, L. M., Haouzi, D., Brothers, G., Penninger, J. M., Peleato, M. L., Kroemer, G., and Susin, S. A. (2001) NADH oxidase activity of mitochondrial apoptosis-inducing factor. *J. Biol. Chem. 276*, 16391−16398.

(9) Lorenzo, H. K., Susin, S. A., Penninger, J., and Kroemer, G. (1999) Apoptosis inducing factor (AIF): a phylogenetically old, caspase-independent effector of cell death. *Cell Death Differ. 6*, 516−524.

(10) Delettre, C., Yuste, V. J., Moubarak, R. S., Bras, M., Robert, N., and Susin, S. A. (2006) Identification and characterization of AIFsh2, a

DOI: 10.1021/acs.biochem.5b00696
Biochemistry 2015, 54, 5175−5184

mitochondrial apoptosis-inducing factor (AIF) isoform with NADH oxidase activity. *J. Biol. Chem. 281*, 18507−18518.
(11) Cheung, E. C., Joza, N., Steenaart, N. A., McClellan, K. A., Neuspiel, M., McNamara, S., MacLaurin, J. G., Rippstein, P., Park, D. S., Shore, G. C., McBride, H. M., Penninger, J. M., and Slack, R. S. (2006) Dissociating the dual roles of apoptosis-inducing factor in maintaining mitochondrial structure and apoptosis. *EMBO J. 25*, 4061−4073.
(12) Sevrioukova, I. F. (2009) Redox-linked conformational dynamics in apoptosis-inducing factor. *J. Mol. Biol. 390*, 924−938.
(13) Sevrioukova, I. F. (2011) Apoptosis-inducing factor: structure, function, and redox regulation. *Antioxid. Redox Signaling 14*, 2545−2579.
(14) Ferreira, P., Villanueva, R., Martínez-Júlvez, M., Herguedas, B., Marcuello, C., Fernandez-Silva, P., Cabon, L., Hermoso, J. A., Lostao, A., Susin, S. A., and Medina, M. (2014) Structural insights into the coenzyme mediated monomer-dimer transition of the pro-apoptotic apoptosis inducing factor. *Biochemistry 53*, 4204−4215.
(15) Senda, T., Yamada, T., Sakurai, N., Kubota, M., Nishizaki, T., Masai, E., Fukuda, M., and Mitsui, Y. (2000) Crystal structure of NADH-dependent ferredoxin reductase component in biphenyl dioxygenase. *J. Mol. Biol. 304*, 397−410.
(16) Senda, M., Kishigami, S., Kimura, S., Fukuda, M., Ishida, T., and Senda, T. (2007) Molecular mechanism of the redox-dependent interaction between NADH-dependent ferredoxin reductase and Rieske-type [2Fe-2S] ferredoxin. *J. Mol. Biol. 373*, 382−400.
(17) Sotres, J., Lostao, A., Gomez-Moreno, C., and Baro, A. M. (2007) Jumping mode AFM imaging of biomolecules in the repulsive electrical double layer. *Ultramicroscopy 107*, 1207−1212.
(18) van GELDER, B., and SLATER, E. C. (1962) The extinction coefficient of cytochrome c. *Biochim. Biophys. Acta 58*, 593−595.
(19) Delano, W. L. (2002) *The PyMOL molecular graphics system*, DeLano Scientific, San Carlos, CA, USA, http://www.pymol.org.
(20) Horcas, I., Fernandez, R., Gomez-Rodriguez, J. M., Colchero, J., Gomez-Herrero, J., and Baro, A. M. (2007) WSXM: a software for scanning probe microscopy and a tool for nanotechnology. *Rev. Sci. Instrum. 78*, 013705.
(21) Sano, S., Tao, S., Endo, Y., Inaba, T., Hossain, M. A., Miyake, C., Matsuo, M., Aoki, H., Asada, K., and Saito, K. (2005) Purification and cDNA cloning of chloroplastic monodehydroascorbate reductase from spinach. *Biosci., Biotechnol., Biochem. 69*, 762−772.
(22) Li, F., Wu, Q. Y., Sun, Y. L., Ma, N. N., Wang, X. Y., and Meng, Q. W. (2010) Evidence that the amino acid residue Cys117 of chloroplastic monodehydroascorbate reductase is involved in its activity and structural stability. *Int. J. Biol. Macromol. 46*, 350−355.
(23) Rinaldi, C., Grunseich, C., Sevrioukova, I. F., Schindler, A., Horkayne-Szakaly, I., Lamperti, C., Landoure, G., Kennerson, M. L., Burnett, B. G., Bonnemann, C., Biesecker, L. G., Ghezzi, D., Zeviani, M., and Fischbeck, K. H. (2012) Cowchock syndrome is associated with a mutation in apoptosis-inducing factor. *Am. J. Hum. Genet. 91*, 1095−1102.
(24) Ghezzi, D., Sevrioukova, I., Invernizzi, F., Lamperti, C., Mora, M., D'Adamo, P., Novara, F., Zuffardi, O., Uziel, G., and Zeviani, M. (2010) Severe X-linked mitochondrial encephalomyopathy associated with a mutation in apoptosis-inducing factor. *Am. J. Hum. Genet. 86*, 639−649.
(25) Berger, I., Ben-Neriah, Z., Dor-Wolman, T., Shaag, A., Saada, A., Zenvirt, S., Raas-Rothschild, A., Nadjari, M., Kaestner, K. H., and Elpeleg, O. (2011) Early prenatal ventriculomegaly due to an AIFM1 mutation identified by linkage analysis and whole exome sequencing. *Mol. Genet. Metab. 104*, 517−520.
(26) Modjtahedi, N., Giordanetto, F., and Kroemer, G. (2010) A human mitochondriopathy caused by AIF mutation. *Cell Death Differ. 17*, 1525−1528.

DOI: 10.1021/acs.biochem.5b00696
Biochemistry 2015, 54, 5175−5184